

Electrostatic force spectroscopy of near surface localized states

Aykutlu Dâna

*Advanced Research Labs, Department of Physics,
Bilkent University, 06800 Ankara, Turkey*

Yoshihisa Yamamoto

Edward L. Ginzton Laboratory, Stanford University, Stanford, California 94305-4085

Abstract

Electrostatic force microscopy at cryogenic temperatures is used to probe the electrostatic interaction of a conductive atomic force microscopy tip and electronic charges trapped in localized states in an insulating layer on a semiconductor. Measurement of the frequency shift of the cantilever as a function of tip-sample shows discrete peaks at certain voltages when the tip is located near trap centers. These discrete changes in frequency is attributed to one by one filling of individual electronic states when the quantized energies traverses the substrate conduction band fermi energy as tip-sample voltage is increased. Theoretical analysis of the experiment suggests that such measurement of the cantilever frequency shift as a function of bias voltage can be interpreted as an AC force measurement, from which spectroscopic information about the location, energy and tunneling times of localized states can be deduced. Experimental results from study of a sample with InAs quantum dots as trap centers is presented.

Keywords:

I. INTRODUCTION

As the semiconductor device size continues to shrink, new methods for characterization of electrical properties of materials and novel devices on the nanometer scale are required [1]. Detection of impurities, characterization of complex material stacks and interfacial properties, non-destructive electrical characterization of ultra-thin gate and capacitor dielectrics and 3D dopant profiling are few of the challenges faced as the device size decreases to nanometer scale. The challenge of electrical characterization of novel devices with smaller number of atoms motivates development of a technique that provides qualitative information about individual electronic states available within the devices.

Since its introduction [2], the atomic force microscope (AFM) and its spin-off techniques have been widely used in imaging and characterization of semiconductor surfaces. Electrostatic force based imaging techniques[3] such as Kelvin probe microscopy (KPM), scanning capacitance microscopy (SCM) and scanning spreading resistance microscopy (SSRM) among others have been used to electrically characterize surfaces. Still, an in-situ, non-destructive technique for characterization of semiconductor surfaces and sub surface structures at the single electronic state level is not available. Because of its high force sensitivity, AFM has been used to detect the presence of individual electronic charges on the sample surface or inside layers near the surface [4, 5, 6]. However, to be able to use the AFM to characterize individual states, we still need to develop a method of obtaining information about the location, energy and dynamics of states on or near the semiconductor surface through force measurements.

In this article, to address this problem, we present a technique based on measurement of electrostatic forces between a conducting AFM tip and charges localized at near-surface electronic states. A conducting AFM tip is used both as a gate electrode and as an electrometer that senses accumulated charge on the sample. Measurement of electrostatic forces between the tip and the sample as a function of the tip-sample bias voltage provide information about the location, energy and tunneling dynamics of localized states. Regarding this measurement technique as a spectroscopy, we refer to it as electrostatic force spectroscopy (EFS) from here on. In the following sections, we begin by formulating the problem, defining the sample structure to which this technique applies, give a theoretical analysis of the EFS experiment, and provide experimental results.

II. THEORETICAL ANALYSIS OF ELECTROSTATIC FORCE SPECTROSCOPY OF LOCALIZED STATES

When biased a conducting AFM tip is brought near a conducting sample surface, due to the finite tip sample capacitance, charges of opposite sign accumulate in the tip and on the sample surface. This electrostatic interaction can be measured through deflection of the cantilever or through perturbation of its resonance frequency. If the sample is a semiconductor or a layered semiconductor/insulator structure with localized states, the electrostatic interaction between the tip and the sample deviates from a simple capacitor and presence of localized states has to be accounted for in the analysis of the electrostatic forces. Based on a model of the sample, measurement of electrostatic interaction as a function of tip location and tip-sample bias voltage can provide data that can be inverted to give information about the location and energy of localized states or doping concentrations. Characterization of electronic states associated with traps inside thin dielectrics, states at semiconductor interfaces, states due to defects and presence of adsorbates are important for the semiconductor technology. Therefore, we choose to restrict ourselves to a metal-insulator-semiconductor configuration with low density of localized states, as described in the following subsection.

A. Tip-Sample configuration for an EFS experiment

The proposed sample configuration is schematically shown in Fig. 1(a). The conductive AFM tip is placed above a insulator-on-conductor structure, with a tip-sample separation of z_{ts} . In an actual experiment, the insulating layer can be a dielectric material deposited or grown on top of the highly conductive region, or a thin dielectric film otherwise placed on a flat conductive sample. In the analysis presented here, the sample is assumed to be a monolithic semiconductor where the conductive region and the insulating dielectric layer is defined by doping. The band diagram in such a configuration is illustrated in Figure 1b. The localized states can be due to impurities, dislocations, interface traps or intentionally introduced states due to presence of quantum dots. The sample structure presented here has certain benefits. The localized states are inside an insulating layer so charge trapped in these states are not screened by free carriers. Also, since there is no doping in the top layer, the 3D potential profile generated by the tip is simple to analyze analytically. Moreover,

the localized states can be charged and discharged by tunneling of carriers from the bulk through the insulator. This modulation of the charge and resulting perturbation of the electrostatic force forms the basis of the proposed detection method.

B. Electrostatic model for calculating local potentials

Analysis of the EFS scheme begins with a model that describes the electrostatic force between the tip and sample and the potential profile inside the insulating layer. The electrostatic problem described by the tip-sample system can be analyzed analytically through a piecewise model of the tip. The charge density on the tip surface and the potential profile in the insulating region can be calculated approximately by modeling the tip as the union of a conic section and a spherical section as shown in Fig. 2. The overall tip-sample capacitance is assumed to be the sum of individual dihedral capacitances[7] formed by infinitesimal surface elements on the tip (shown as location A in Fig. 2) and corresponding surface elements on the surface (location B in Fig. 2).

The sphere-cone model of the tip can be used to estimate the local potential $V(x, z)$ (see Fig. 2) inside the insulating layer. The calculation of $V(x, z)$ can be done, by noting that coordinate x is related to the geometrical model variable φ by a single valued function $g(\varphi)$ as

$$x = g(\varphi) = r \sin \varphi + \frac{1 - \cos \varphi}{\sin \varphi} \times [z_{ts} + r(1 - \cos \varphi)]. \quad (1)$$

The local potential $V(x, z)$ is then given by

$$V(x, z) = \frac{V_{ts} z}{\epsilon_r} \times \left[\frac{\varphi [z_{ts} + r(1 - \cos \varphi)]}{\sin \varphi} + \frac{d_{ins}}{\epsilon_r} \right]^{-1} \quad (2)$$

where $\varphi = g^{-1}(x)$. Eq. (2) agrees with a finite element analysis solution of the potential within %5 if $d_{ins}/\epsilon_r \ll z_{ts}$ and $r, z_{ts} \lesssim r$ and $|x| \lesssim 4r$.

For a flat metal sample, the electrostatic force estimated through this model (sphere-cone model) can be expressed in terms of the tip length H_{tip} , tip radius r , tip-sample separation z_{ts} , and tip half-cone angle θ_0 as the sum of conical and spherical contributions

$$F_{sc} = F_{sphere} + F_{cone} \quad (3)$$

where the spherical and conical terms are given by

$$F_{sphere} = V_{ts}^2 \pi \epsilon_0 r^2 \frac{1 - \sin \theta_0}{z_{ts} [z_{ts} + r(1 - \sin \theta_0)]} \quad (4)$$

$$F_{cone} = \frac{V_{ts}^2 \pi \epsilon_0 \sin^2 \theta_0}{(\pi/2 - \theta_0)^2} \times \left[\ln \frac{H_{tip}}{z_{ts} + r(1 - \sin \theta_0)} - 1 + \frac{r \tan \theta_0}{z_{ts} + r(1 - \sin \theta_0)} \right]. \quad (5)$$

The validity of this model can be tested through measurements of force gradients of a biased tip as a function of the tip sample separation. It is seen from the data presented in Fig. 3 that by fitting the tip radius only, the model given in Eq. (3) predicts the tip-sample capacitance qualitatively with less than %5 error in the range $r/2 \lesssim z_{ts} \lesssim 4r$.

C. Model for charging of the localized states

For a given tip-sample geometry, and a given bias voltage V_{ts} , the energy of a localized state i , away from the tip axis a distance x and at a height h_i from the ground plane (see Fig. 1 and Fig. 2) is given by

$$E_i = E_{i,0} - eV(x, h_i) \quad (6)$$

where e is the electronic charge, $V(x, h_i)$ is given by Eq. (2) and $E_{i,0}$ is the energy of the state under zero bias. For a given sample, if we define the dimensionless parameter $\alpha(x, z_{ts})$ as

$$\alpha(x, z_{ts}) = \frac{z + d_{ins}/\epsilon_r}{\varphi(z_{ts} + r(1 - \cos \varphi))/\sin \varphi + d_{ins}/\epsilon_r} \quad (7)$$

where φ is related to x through Eq. (1), we can rewrite Eq. (6) as

$$E_i = E_{i,0} - \frac{eV_{ts}h_i}{z_{ts}\epsilon_r + d_{ins}}\alpha(x, z_{ts}). \quad (8)$$

It worth noting that, for states on the tip axis, $\alpha(0, z_{ts}) = 1$ and Eq. (8) reduces to a simple voltage divider.

In thermal equilibrium, charge q_i of state i can be calculated through thermal statistics as

$$q_i = -\frac{e}{1 + \exp[(E_i - E_f)/k_B T]} \quad (9)$$

where $k_B T$ is the thermal energy.

When E_i is modulated in time, if the tunneling time Γ_i^{-1} is finite but does not strongly depend on V_{ts} , the time dependent charge \tilde{q}_i can be calculated through a first order differential equation as

$$\Gamma_i^{-1} \frac{d\tilde{q}_i}{dt} = -\tilde{q}_i + q_i(t). \quad (10)$$

Here $q_i(t)$ denotes q_i calculated through Eq. (9), and the time dependence is due to modulation of V_{ts} or z_{ts} . Γ_i stands for the tunneling rate for state i for the given DC bias condition. The approximation presented in Eq. (10) would be valid only for a small signal modulation of the charge, since Γ_i depends exponentially on the potential barrier and can not be assumed constant over a large modulation of the barrier. If a small signal sinusoidal modulation of V_{ts} or z_{ts} with frequency ω is present, \tilde{q}_i will be given by a sinusoid that has a phase ϕ that depends on the modulation frequency and tunneling rate Γ_i as

$$\phi = -\arctan(\omega/\Gamma_i). \quad (11)$$

The modulated charge amplitude \tilde{q}_i can be calculated through

$$\tilde{q}_i = \langle \frac{\partial q_i}{\partial V_{ts}} \rangle \tilde{V}_{ts} + \langle \frac{\partial q_i}{\partial z_{ts}} \rangle \tilde{z}_{ts} \quad (12)$$

where the derivatives are calculated through Eqs. (2), (6) and (9), averages denoted by brackets are taken over the modulation ranges of respective modulated variables. Here \tilde{V}_{ts} and \tilde{z}_{ts} are the modulation amplitudes of bias and tip-sample separation respectively.

D. Electrostatic force model in the presence of localized states

The electrostatic interaction of the tip and the ground plane can be analyzed through the sphere-cone model accurately. In the presence of localized states with charges q_i , there is additional contribution to the force from individual charges. For the sake of simplicity, the electrostatic force F_e that includes contributions from the localized charges and the background will be approximated by a parallel plate capacitor model given by [6]

$$F_e \cong \frac{\epsilon_r^2 \xi}{(\epsilon_r z_{ts} + d_{ins})^2} \times \left[\frac{\pi r^2 \epsilon_0 V_{ts}^2}{2} + \sum_i \frac{2h_i q_i V_{ts}}{\epsilon_r} \right] \quad (13)$$

where ξ is a geometric correction factor that can be calculated by equating F_e of Eq. 13 with all q_i being identically zero, to the electrostatic force of Eq. (3). In the parameter range $r/4 < z_{ts} < 2r$, ξ varies from 0.9 to 4.2 being equal to 1 if $z_{ts}/r = 0.4$. It is important to note that Eq. (13) is written assuming that the interaction is due to localized charges on the tip axis and a lumped charge due to tip-sample capacitance concentrated at the tip apex. In reality, force due to each localized state has to be corrected by integrating the force between q_i and the charge distribution on the tip. Also, extension of Eq. (13) to

include effect of charges away from the tip axis can be done by including effect of geometry. The simplification made in derivation of the force in Eq. (13) assuming a lumped parallel plate capacitor model, will have effect only on the magnitude of the forces from individual charges.

E. Modulation of electrostatic force: localized state signatures

When an AC modulation of the tip-sample separation or tip-sample bias voltage is present, Eq. (13) can be used to estimate the AC modulated electrostatic force. Since the objective of EFS experiment proposed in this work is to extract information about localized states through measurement of forces, in this subsection we will analyze the contribution from the localized states only. The AC force due to localized states can be calculated through

$$\tilde{F}_e = \sum_i \frac{\partial F_e}{\partial q_i} \tilde{q}_i \quad (14)$$

where F_e and \tilde{q}_i are given by Eqs. (13) and (10) respectively. Eq. (14) includes only the contribution due to modulation of the charges in the localized states and does not account for the modulated background force due to presence of the bulk of the sample. The background contribution can be calculated by direct differentiation of Eq. (13) with respect to z_{ts} or V_{ts} with q_i set to zero. This background contribution will be analyzed in the following subsections, since it proves to be a significant effect in the detection process.

Each term in the sum on the right-hand side of Eq. (14) contains information about the corresponding localized state, and we shall refer to it as the *signature* of that particular state. The signature force is a function of V_{ts} , the tip location with respect to the sample z_{ts} , the energy of the state $E_{i,0}$ and its height from the ground plane h_i . Therefore, measuring the modulated force for a set of values of V_{ts} and z_{ts} we can estimate $E_{i,0}$ and h_i .

When only a modulation of the bias voltage \tilde{V}_{ts} is present, and tip location is fixed $\tilde{z}_{ts} = 0$, the signature for state i is

$$\tilde{F}_{e,i} = \frac{2\epsilon_r h_i \xi V_{ts}}{(\epsilon_r z_{ts} + d_{ins})^2} \left\langle \frac{\partial q_i}{\partial V_{ts}} \right\rangle \tilde{V}_{ts}. \quad (15)$$

Conversely, when tip-sample separation is modulated only and $\tilde{V}_{ts} = 0$, the signature is

$$\tilde{F}_{e,i} = \frac{2\epsilon_r h_i \xi V_{ts}}{(\epsilon_r z_{ts} + d_{ins})^2} \left\langle \frac{\partial q_i}{\partial z_{ts}} \right\rangle \tilde{z}_{ts}. \quad (16)$$

The dependence of the signatures in Eqs. (15) and (16) on V_{ts} and z_{ts} is presented in Figs. 4 and 5, for a set of typical experimental parameters. It is seen from Fig. 4 that, each state appears as a distinct peak when we plot \tilde{F}_e against V_{ts} . This can be intuitively understood noting that, as the bias voltage is increased, the energy of the state traverses the fermi energy of the ground plane and it is charged. Only when the state energy is close to the fermi energy, the state charge can be modulated by a modulation of the local potential. This modulation amplitude has the energy dependence of the derivative of the thermal distribution and thus the AC force amplitude appears as a peak when plotted versus V_{ts} . The signature voltage $V_{s,i}$ at which the force has peak amplitude is given through Eq. (8) for a state a distance x away from the tip axis as

$$V_{s,i} = \frac{E_{i,0}(\epsilon_r z_{ts} + d_{ins})}{eh_i \alpha(x, z_{ts})} \quad (17)$$

and in the limit of infinitesimal modulation amplitude, the width $\Delta V_{s,i}$ of the peak in terms of bias voltage is

$$\Delta V_{s,i} = \frac{2k_B T(\epsilon_r z_{ts} + d_{ins})}{eh_i \alpha(x, z_{ts})}. \quad (18)$$

It is noted from Fig. 4 that, as the temperature is decreased and $k_B T$ becomes small compared to the modulation of E_i , the averaging of the derivative of q_i (denoted by the brackets in Eqs. (15) and (16)) over the modulation range causes the signature to deviate from a gaussian-like peak, and Eq. (18) no longer applies.

If $\Delta V_{s,i}$ can be measured accurately, then we can estimate $E_{i,0}$ from Eqs. (17) and (18) as

$$E_{i,0} = \frac{2k_B T V_{s,i}}{\Delta V_{s,i}}. \quad (19)$$

To reduce the error in estimation of state parameters, one can repeat the EFS measurement changing only the tip location. From a set of EFS data taken at different values of the z_{ts} , it is possible to determine $V_{s,i}$, $\Delta V_{s,i}$ and $\partial V_{s,i} / \partial z_{ts}$. These parameters can then be used to solve for the three unknowns x , $E_{i,0}$ and h_i through Eqs. (17), (18) and (19) uniquely.

In a case where measurement of $\Delta V_{s,i}$ has large error bounds due to imperfections of the measurement setup, another method has to be devised to extract location, height and energy of the state. Due to the cylindrical symmetry of the tip, the potential of Eq. (2) will have circular equipotential contours. If the tip is scanned in the x - y plane keeping V_{ts} and z_{ts} constant, and $V_{s,i}$ is plotted as a function of x and y , resulting image will exhibit circular

patterns whose radii can be related to the experimental parameters and parameters of the state i using Eq. (17). The data resulting from such a measurement can also be used to estimate h_i as will be illustrated in the experimental sections.

F. Measurement of electrostatic forces: Self-oscillation technique

The electrostatic force, modulated or DC, causes a deflection of the cantilever which can then be detected through a secondary detector, such as a laser interferometer. The minimum detectable electrostatic force is given by the thermomechanical noise limit, regardless of measurement frequency or technique. However, modulation frequency or measurement technique can be important in optimization of the signal-to-noise ratio (SNR), since secondary detector can not be assumed noiseless. For example, a typical laser interferometer used for cantilever deflection detection in our experiments, has a noise floor of $2 \times 10^{-3} \text{ \AA}/\sqrt{\text{Hz}}$. Referring to the figure 4 and 5, modulated electrostatic forces due to single states are on the order of 10^{-12} Nt for a typical experimental configuration. If a cantilever with a spring constant of say $k_0=1 \text{ Nt/m}$ and quality factor $Q \sim 10^4$ is used, the peak deflection amplitude for a state signature will be on the order of 10^{-12} m if modulation frequency is near DC and 10^{-8} m if modulation frequency ω is on resonance with the cantilever mechanical resonance ω_0 . The secondary detection limited charge sensitivity can be estimated to be $0.1 \text{ e}/\sqrt{\text{Hz}}$ near DC and $10^{-5} \text{ e}/\sqrt{\text{Hz}}$ on resonance. However, thermomechanical noise floor for our cantilevers is $4 \times 10^{-16} \text{ Nt}/\sqrt{\text{Hz}}$ at 4 K independent of ω , and it corresponds to a fundamental limit for charge resolution of $4 \times 10^{-4} \text{ e}/\sqrt{\text{Hz}}$. Thermomechanical noise is dominant in the overall force measurement if $\omega \simeq \omega_0$.

Modulation frequency and technique is also important in realization of the EFS experiment. In order for the analysis presented for the modulation of V_{ts} to hold, z_{ts} must be kept constant, otherwise Eq. (15) will no longer describe the signature force correctly. In practice, this can be done by suppression of the cantilever oscillation by a feedback loop. However, modulation of the bias voltage with $\omega \simeq \omega_0$ requires tracking of the frequency shift of the cantilever due to the z-gradient of the background electrostatic force which is given by

$$\Delta\omega = -\frac{\omega_0 \xi \pi \epsilon_r^3 \epsilon_0 r^2 V_{ts}^2}{2k_0(\epsilon_r z_{ts} + d_{ins})^3} \quad (20)$$

where k_0 is the spring constant of the cantilever.

The difficulties one has to overcome in order to realize the EFS experiment by modulating V_{ts} can be solved if z_{ts} is modulated instead of V_{ts} . Modulation of z_{ts} has the two benefits: First, there is no need actively to suppress modulation of V_{ts} to validate assumptions made in analysis, since it can be biased by an external DC voltage source. Second, if the cantilever is oscillated by positive feedback or a phase-locked loop system on its resonance, the modulation of z_{ts} will automatically be always on resonance with the cantilever. These benefits motivate the use of self-oscillation of the cantilever.

Technical description of self-oscillation feedback can be found elsewhere[8, 9]. Self-oscillation technique was generally used to detect the force gradients due to time invariant interactions. This method can be applied to measurement of AC forces through frequency shift measurements. The method uses feedback to sustain the oscillation of the cantilever on its resonance, by measuring the AC deflection \tilde{z}_{ts} , phase shifting by $\pi/2$, conditioning it for amplitude control and feeding it back as a drive force \tilde{F}_D . The effect of the external feedback can be written by setting $\tilde{z}_{ts}(t) = \tilde{z}_{ts} \sin(\omega t)$ and $\tilde{F}_D(t) = \tilde{F}_D \cos(\omega t)$. When an external signal force $\tilde{F}_s(t) = \tilde{F}_s \sin(\omega t + \phi)$ is present, the oscillation amplitude \tilde{z}_{ts} and oscillation frequency $\delta\omega$ can be calculated through

$$\tilde{z}_{ts} \cong \frac{Q}{k_0}(\tilde{F}_D + \tilde{F}_s \sin \phi) \quad (21)$$

and

$$\delta\omega \cong \frac{\omega_0}{2k_0\tilde{z}_{ts}}\tilde{F}_s \cos \phi \quad (22)$$

where Q is the quality factor of the cantilever. Approximations presented in Eqs. (21) and (22) can be assumed valid if $\delta\omega \ll \omega_0$.

Inserting $\tilde{F}_s = \tilde{F}_{e,i}$ from Eq. (16), the signature of a state can be measured in the frequency shift of the cantilever in self-oscillation configuration as

$$\delta\omega_i = \frac{\omega_0 \epsilon_r h_i \xi V_{ts} \cos \phi}{k_0 (\epsilon_r z_{ts} + d_{ins})^2} \left\langle \frac{\partial q_i}{\partial z_{ts}} \right\rangle. \quad (23)$$

The effect of temperature and oscillation amplitude on the overall SNR for this measurement scheme is illustrated in Fig. 6. The phase ϕ can be estimated by measuring \tilde{z}_{ts} and $\delta\omega_i$ for a single state. Tunneling rate Γ_i for the state can then be related to ϕ through Eq. (11).

In the self-oscillation method based measurement of the signatures, the total frequency shift is the sum of the background frequency shift of Eq. (20) and signature frequency shifts given by Eq. (23) as

$$\Delta\omega_{efs} = \Delta\omega + \sum_i \delta\omega_i \quad (24)$$

The minimum detectable charge in the frequency shift method is again given by the thermomechanical detection limit although method of detection is through measurement of frequency shift instead of deflection. Also, presence of the self-oscillation feedback does not affect the value of minimum detectable force. Only difference is, force noise translates to a fundamental frequency noise

III. EXPERIMENT

The EFS experiments presented here uses a home built low temperature AFM system that can operate down to 4.2 K. A fiber interferometer serves as the secondary detector. The laser wavelength is $\lambda=1310$ nm, with $100 \mu\text{W}$ optical power incident on the cantilever, and measured noise floor for deflection detection is $2 \times 10^{-3} \text{ \AA}/\sqrt{\text{Hz}}$. Commercial Pt/Ir coated cantilevers with spring constants of $k_0=2.8 \text{ Nt/m}$ and resonant frequencies of $\omega_0=75 \text{ KHz}$ are used. Supplier specified tip lengths are $H_{\text{tip}} \simeq 10 \mu\text{m}$ and the half-cone angle of the tip is 20° . The tip radius is not specified but can be extracted through force measurements to be $r \simeq 20 \text{ nm}$. The quality factor of the cantilevers Q is around 150 in air, 15,000 at room temperature in vacuum, and range from 30,000 to 45,000 as temperature is decreased from 77.3 K to 4.2 K. Mechanical actuation of the cantilever oscillation using a piezoelectric element can produce spurious frequency shifts because mechanical structures can have multiple resonances near the operation frequency. Therefore, an electrostatic actuation scheme is used to oscillate the cantilever because of constant phase and amplitude response in the frequency range of interest.

The sample is chosen to contain InAs QDs embedded in insulating GaAs since similar samples have been previously extensively studied for characterization of QD energy levels by optical and electrical methods[10, 11]. Based on previous capacitance spectroscopy experiments [12] incorporating similar InAs QDs, we expect the QD energies to be from 250 meV to 100 meV below the GaAs conduction band edge. It is also estimated that the number

of confined energy levels and values of confined energies depend on QD size and up to 12 confined energy levels are estimated as the QD base diameter approaches 40 nm. Growth conditions have a strong effect on QD energy levels [10, 13] since gallium can replace indium in the dots and this alloying affects QD band gap. Although it is not possible to know the quantized energies of QDs only knowing the growth conditions, a rough estimation of the energy levels is still important for choosing the right experimental parameters of tip-sample separation and bias voltage range.

The sample is a molecular beam epitaxy (MBE) grown GaAs structure. First, a GaAs buffer layer with silicon doping of density 10^{18} cm^{-3} and thickness of 500 nm is grown, followed by an undoped GaAs layer of 15 nm thickness. Then a monolayer of InAs wetting layer was grown followed by a single layer of InAs QDs. The dots were capped by a undoped GaAs capping layer of 15 nm thickness. Topographical AFM image of a test sample grown under same conditions without capping layer, the QDs were found to be about 20 nm in diameter, about 4 nm tall, with a surface density of 10^{10} cm^{-2} .

Contact mode topographic images of the surface was obtained prior to the EFS experiment to ensure the flatness and cleanliness of the surface. Force-distance curve with $V_{ts}=0\text{V}$ provides information about the location of the surface, z_s . The drift of the scanner in x,y and z directions were characterized by repeating imaging and force-distance measurements with few minutes intervals, before and after the experiments. It was seen that when the AFM is operated at 4 K, the drift was insignificant ($\sim 2 \text{ nm}$) over an hour and can be ignored.

A. Observation of the wetting layer

It is known through previous experiments[10] that the InAs wetting layer (WL) forms a 2 dimensional electron gas (2 DEG). In a crude approximation, it can be regarded as a collection of localized states and should present some form of signature in the EFS data. Study of charging of the WL in our EFS experiment is interesting, since it produces a large signal due to large number of electronic states. Also, the ground state energy of the WL with respect to the GaAs conduction band edge can provide a reference for the EFS data. Finally, the WL provides states at all locations on the sample and we do not have to find a proper location to observe the WL. The band gap of GaAs at room temperature is $E_{\text{GaAs}}=1.52 \text{ eV}$ at 4.2 K, and surface pinning is assumed to be at the middle of the band gap.

In previous photoluminescence measurements of similar structures, WL optical transition occurs 1.42 eV. Therefore, if we assume for the sake of interpretation of EFS data, that WL is a localized state, the corresponding electron energy for that state under zero bias condition will be $E_{wl,0} = 330$ meV. The EFS data shown in Fig. 7 is collected with a tip sample separation of $z_{ts}=14.5$ nm, where z_{ts} is measured by a force-distance curve. A sudden change in the frequency shift indicates presence of states that is charged when $V_{ts}=5.83$ V. EFS experiment is repeated at different tip-sample separations to fit the height h_{wl} and $E_{wl,0}$, and we find that $h_{wl}=14$ nm, $E_{wl,0}=360$ meV (shown in inset of Fig. 7). The discrepancy of EFS results may be due to pinning of the GaAs surface at a slightly different energy than the middle of band gap, or due to the fact that any band-bending effects were ignored in our model.

B. Observation of localized states

In the EFS experiments performed with the aim of identifying QD energy levels, based on theoretical calculations and preliminary information given by the observation of WL, choosing z_{ts} to be around 20 nm and \tilde{z}_{ts} to be less than 1 nm, we expect to obtain a SNR greater than 10 in a 100 Hz bandwidth for single states. In the capped sample, it is not possible to locate the dots through topographical imaging since the capping produces a flat surface. Therefore, EFS experiments were performed on a grid of points on a flat region of the sample.

Observation of isolated single signatures depends on presence of isolated single states in the sample. If there are many states in the close vicinity of the tip, it is hard to distinguish individual peaks from a single EFS measurement. This fact is illustrated by Fig. 8(a), where many charging signatures can be seen between $-4.5V < V_{ts} < -2.8V$. It is also seen that as z_{ts} moves from 19 nm to 20 nm, the peaks appear at a slightly more negative voltage range $-4.9V < V_{ts} < -3V$ as expected from Eq. (17). Although this expected behaviour of states shifting towards stronger biases can be observed, because of large number of superimposed peaks it is not possible to identify individual signatures unambiguously. A single isolated state signature from an EFS measurement performed at a different location, shown in Fig. 8(b), features a single isolated signature. For this state, $V_{s,i}$ also shifts towards negative voltages as z_{ts} moves from 30 nm to 35 nm. Since this signature is well isolated, it is

possible to estimate the energy and depth of the state. Based on Eqs. (17), (18) and (19), we can estimate this state parameters to be, $E_{i,0} = 0.105$ eV, $h_i = 14$ nm and located $x = 51$ nm from the tip axis.

Fig. 9(a) is an example of EFS data with no signatures of localized states. Slowly varying background forces due to the presence of ground plane were fitted and subtracted to clarify that there are no distinct peaks. Fig. 9(b) shows EFS data for another location on the sample, with six distinct peaks in both frequency shift and oscillation amplitude. Similar signatures can also be observed near a QD in a sample grown exactly the same but without a capping layer (Fig. 9(c)). In the uncapped sample the signatures disappear when the tip is moved away from the QD, demonstrating that the signatures are indeed due to the QD. Energies can be fitted to each peak. The energies estimated from Fig. 9(b), 9(c) and energies measured through conventional capacitance spectroscopy for similar dots in a previous measurement[11] are compared in Table 1.

To further illustrate the effect of tip location on $V_{s,i}$ one can plot the signature amplitude as a function of x and y in the vicinity of a localized state. Three signatures appear at a bias of -4.45 V (Fig. 10(a)) and as the voltage is increased to -5.15 V (Fig. 10(b)), the location of the signature peak defines a circular pattern, equivalent to an equipotential contour which is defined by Eq. (6). Energy and height of the state can be estimated as $h_i = 14.5$ nm and $E_{i,0} = 205$ meV by fitting Eq. (6) to the data.

IV. CONCLUSIONS

A simplified theory of EFS generalized to a family of samples that has localized states inside a thin insulating layer is presented. The technique is capable of extracting information about individual localized states with nanometer resolution and 4×10^{-4} electronic charge sensitivity. Application of the technique to InAs quantum dots embedded in a semiinsulating GaAs matrix is presented as a demonstration. The presented theory gives guidelines for choice of cantilever and sample parameters for a given application of EFS. Potential applications include, high resolution 3D dopant profiling in semiconductors, characterization of novel thin gate dielectrics, and nondestructive characterization of self-assembled monolayer materials for nanoelectronic devices.

Acknowledgments

The authors would like to thank JST and Stanford University for their continued support during this work.

- [1] The International Technology roadmap for Semiconductors - Metrology, published by International Forum on Semiconductor Technology (2001).
- [2] G. Binnig, C.F. Quate, C. Gerber, Phys. Rev. Lett. **56**, 930 (1986).
- [3] P. De Wolf, R. Stephenson, T. Trenkler, T. Clarysse, T. Hantschel, and W. Vandervorst, J. Vac. Sci. Technol. B **18**, 361 (2000).
- [4] D. M. Schaadt, E. T. Yu, S. Sankar and A. E. Berkowitz, Appl. Phys. Lett. **74**, 472 (1999).
- [5] J. T. Jones, P. M. Bridger, O. J. Marsh, and T. C. McGill, Appl. Phys. Lett. **75**, 1326 (1999).
- [6] L. J. Klein and C. C. Williams, Appl. Phys. Lett. **79**, 1828 (2001).
- [7] S. Hudlet, M. Saint Jean, C. Guthmann, J. Berger, Euro. Phys. J. B **2** 5 (1998).
- [8] T. R. Albrecht, P. Grtter, D. Horne, and D. Rugar, J. Appl. Phys. **69**, 668 (1991).
- [9] U. Drig, H. R. Steinauer and N. Blanc, J. Appl. Phys. **82**, 3641 (1997).
- [10] J. M. Garca, T. Mankad, P. O. Holtz, P. J. Wellman, and P. M. Petroff, Appl. Phys. Lett. **72**, 3172 (1998).
- [11] R. J. Luyken, A. Lorke, A. O. Govorov, J. P. Kotthaus, G. Medeiros-Ribeiro and P. M. Petroff, Appl. Phys. Lett. **74**, 2486 (1999).
- [12] G. Medeiros-Ribeiro, F. G. Pikus, P.M. Petroff, and A. L. Efros, Phys. Rev. B **55**, 1568 (1981).
- [13] T. M. Hsu, Y. S. Lan, W.-H. Chang, N. T. Yeh and J.-I. Chyi, Appl. Phys. Lett. **76**, 691 (2000).

TABLE I: Electron energy levels inferred from previous capacitive measurements for 20 nm base diameter capped dots[?], theory for 11.3 nm base diameter capped dots[?] and this experiment involving 40 nm base diameter uncapped dot. Electron energies are shifted to match the ground state energies, E_{s-1} . The calculation by Kim et al. [?] does not take into account Coulomb charging effects and estimates E_{s-1} to be 231 meV below the GaAs conduction band minimum.

Energy level	Theory	Capacitance data	EFS for capped QD
E_{s-1} (meV)	0	0	0
E_{s-2} (meV)		19	35
E_{p-1} (meV)	84	74	57
E_{p-2} (meV)		82	63
E_{p-3} (meV)	111	100	88
E_{p-4} (meV)		110	93

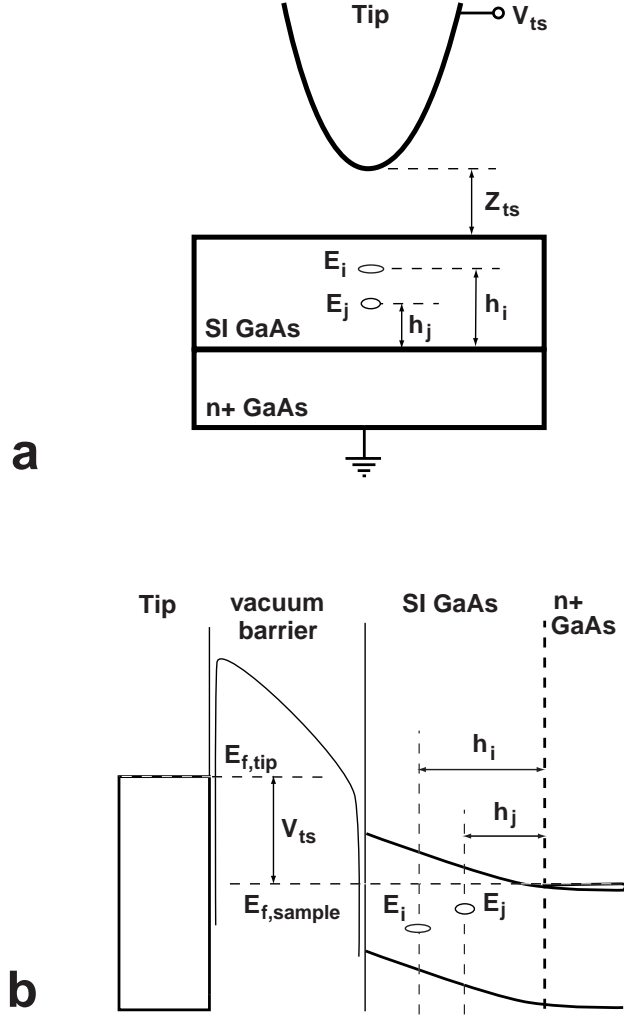


FIG. 1: Schematic of the EFS experiment. a, Configuration of the tip and the sample that contains the states to be studied. States with energies E_i at heights h_i are located inside an insulating layer on top of a highly conductive ground plane. In the analysis and experiments presented in this work, the sample is chosen to be a monolithic semiconductor. The insulating and conducting regions are determined by doping. b, Illustration of the energy band diagram.

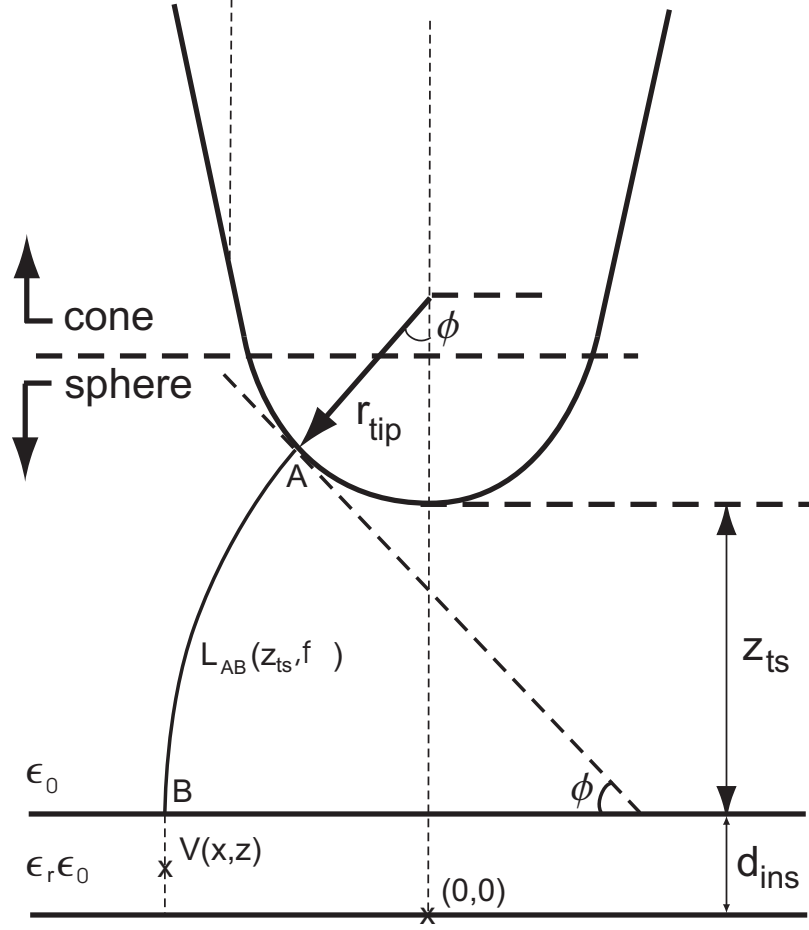


FIG. 2: Description of the sphere-cone model of the tip-sample interaction. The AFM tip is modelled as the union of spherical and conical sections. The electrostatic problem is solved by integrating contributions of individual dihedral capacitors formed between surface elements on the tip (point A) and corresponding surface elements on the sample (point B). Tip-sample electrostatic force and potential profile inside the dielectric ($V(x, z)$) can be accurately described by the model.

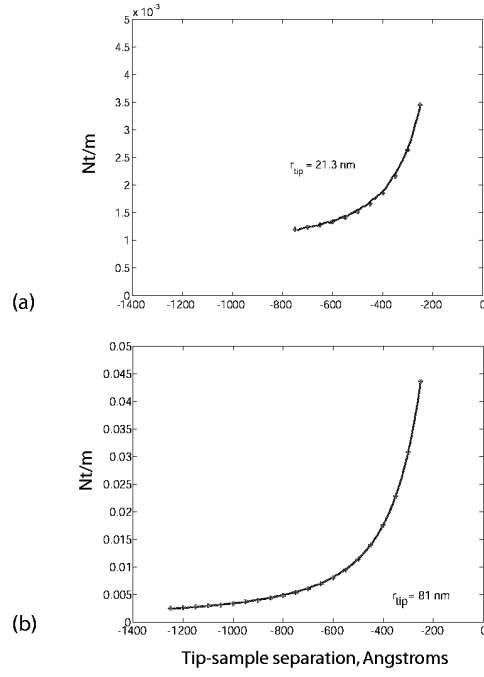


FIG. 3: Electrostatic force gradient $\partial F_e/\partial z$ measured through frequency shift of the cantilever and theoretical estimation through Eq. 3 by fitting the tip radius. a) A fresh tip has a fitted radius of $r = 21.3$ nm. b) After contact imaging and deposition of metal on the surface through pulsing of the bias voltage, the tip radius increases to $r = 81$ nm.

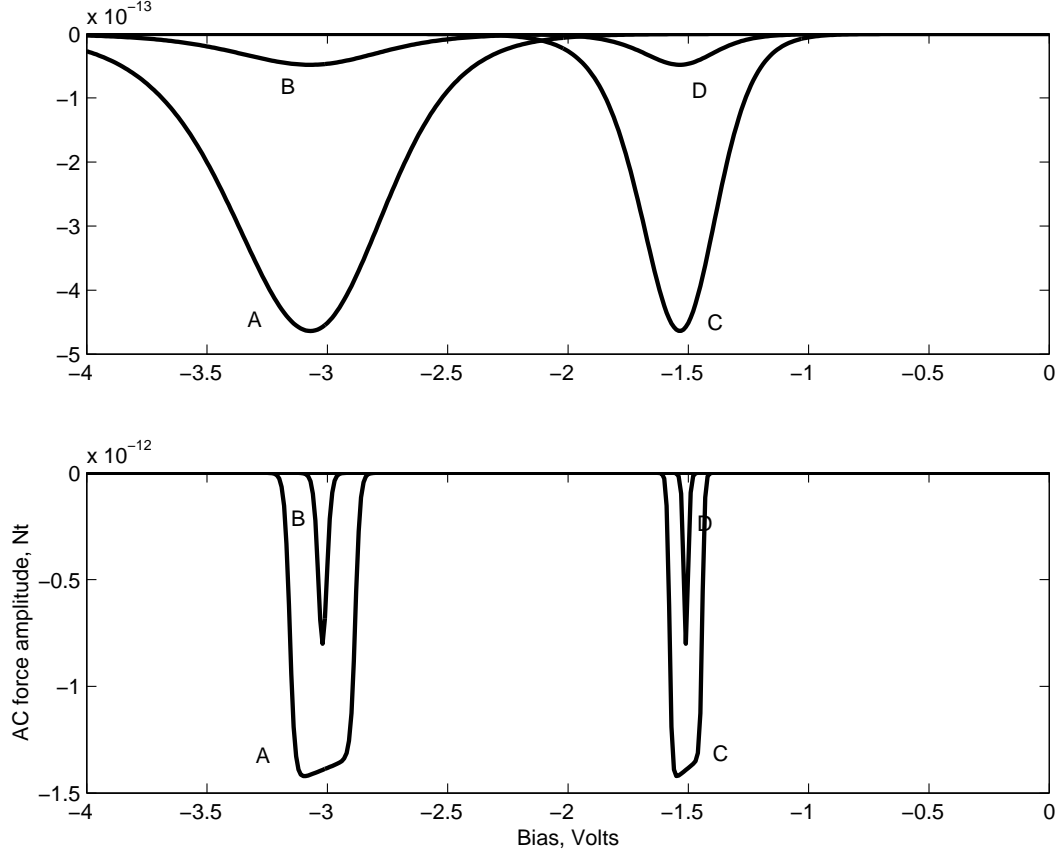


FIG. 4: Theoretical force signatures of two states, a) under modulation of the tip-sample separation at $T=77$ K. Curves A and B are calculated for a state with the parameters $E_{i,0}=0.1$ eV, $h_i=10$ nm, with modulation amplitude $\tilde{z}_{ts} = 1$ nm and 0.1 nm respectively. Curves C and D are for a state with the parameters $E_{i,0}=0.1$ eV, $h_i=20$ nm. b) Same as (a) except $T=4$ K. The voltage at which the force peak occurs, and the width of the peak in terms of bias voltage provide information about energy and location of the state. The sample is chosen to be GaAs, with $\epsilon_r = 13.6$. Thickness of the insulating section is $d_{ins} = 30$ nm. Tip radius is $r=20$ nm and $z_{ts} = 20$ nm. Negative amplitudes denote the fact that the modulated force has opposite phase with the modulation of the tip-sample separation.

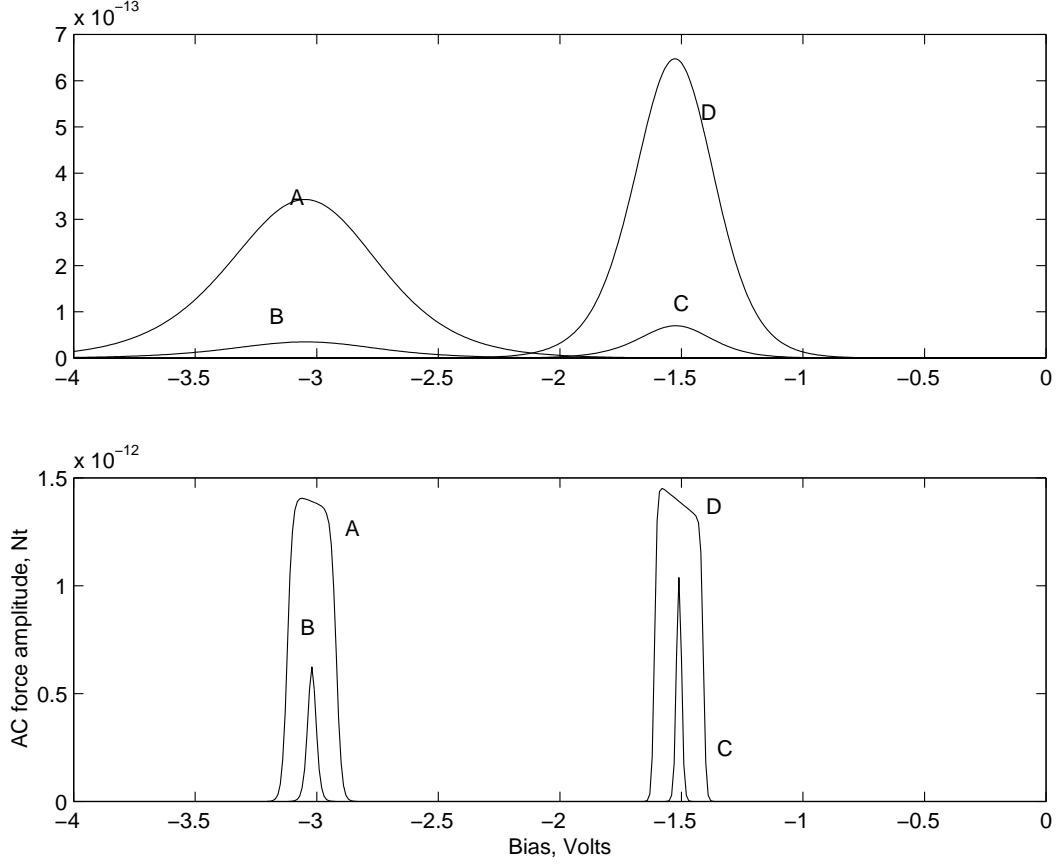


FIG. 5: Theoretical force signatures of two states, a) under modulation of the bias voltage V_{ts} at $T=77$ K. Curves A and B are calculated for a state with the parameters $E_{i,0}=0.1$ eV, $h_i=10$ nm, with modulation amplitude $\tilde{V}_{ts} = 10$ mV and 100 mV respectively. Curves C and D are for a state with the parameters $E_{i,0}=0.1$ eV, $h_i=20$ nm. b) Same as (a) except $T=4$ K. Sample parameters are the same as in Figure 4. Positive amplitudes denote the fact that the modulated force has same phase with \tilde{V}_{ts} .

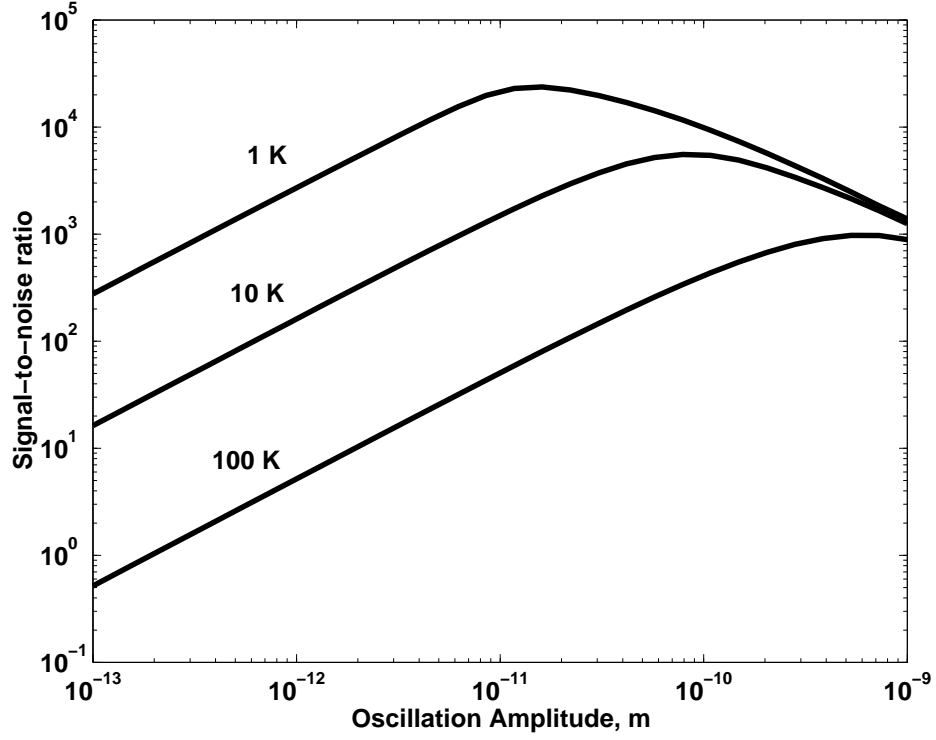


FIG. 6: Signal-to-noise ratio for a single localized state in the frequency measurement technique as a function of temperature and oscillation amplitude \tilde{z}_{ts} . The state parameters are $E_{i,0}=350$ meV, $h_i=14$ nm. Total dielectric thickness is $d_{ins}=30$ nm and $\epsilon_r=13.6$. Cantilever resonance frequency is $\omega_0/2\pi=73$ KHz, and spring constant is $k_0=2.8$ Nt/m. Tip sample separation is $z_{ts}=12$ nm. Frequency detection is limited by noise of the electronics at higher oscillation amplitudes. This fact causes SNR to decrease if the oscillation amplitude is increased above an optimal value which is about 1 Å at 10 K.

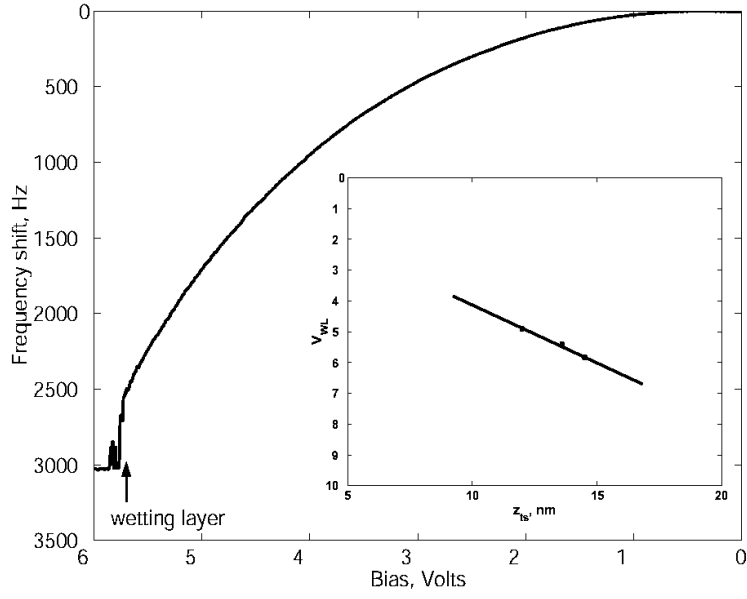


FIG. 7: Observation of the InAs wetting layer (WL). The frequency shift due to background electrostatic forces follows a parabola which shows a sudden jump, indication of presence of a large number of states. Inset shows theoretical estimation of the signature voltage V_{wl} as a function of z_{ts} . Fitting to data, the states which cause the jumps is estimated to be $h_{wl} = 14$ nm above the ground plane and at an energy 25 meV below the GaAs conduction band.

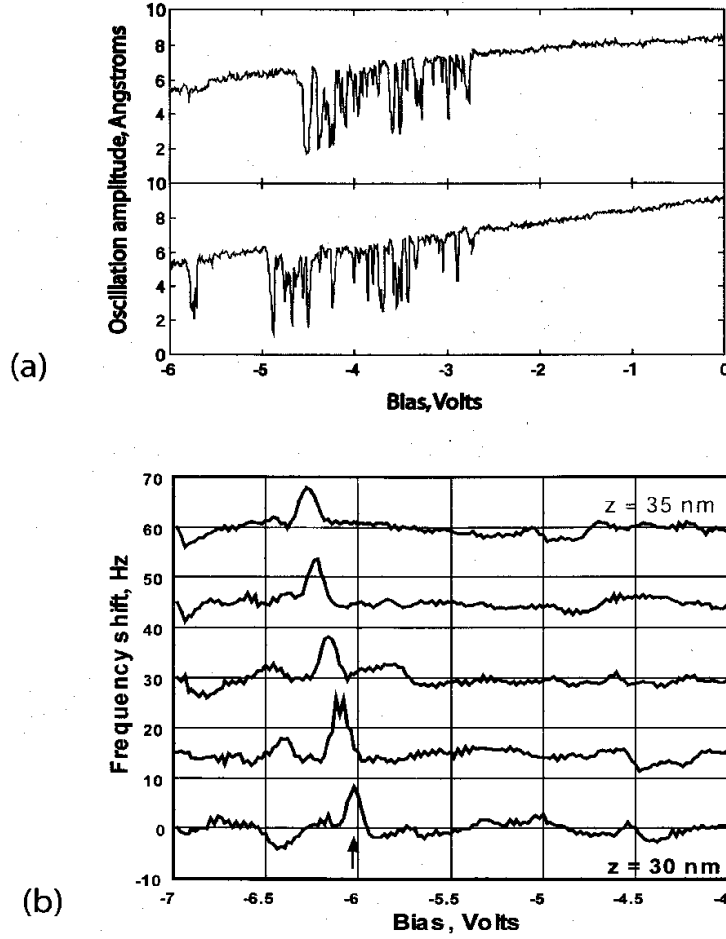


FIG. 8: Observation of localized states. a) Multiple signature peaks appear in the oscillation amplitude of the cantilever, in the bias voltage range $-4.5\text{V} < V_{ts} < -2.8\text{V}$ when $z_{ts}=19$ nm (top curve). As the tip is moved away from the sample, to $z_{ts}=20$ nm, signature peaks move to stronger bias voltages $-4.9\text{V} < V_{ts} < -3.0\text{V}$ (bottom curve). b) A single state signature can be isolated in the EFS data taken at a different location of the sample. Signature voltage $V_{s,i}$ moves to stronger biases as the tip-sample separation z_{ts} is increased from 30 nm to 35 nm.

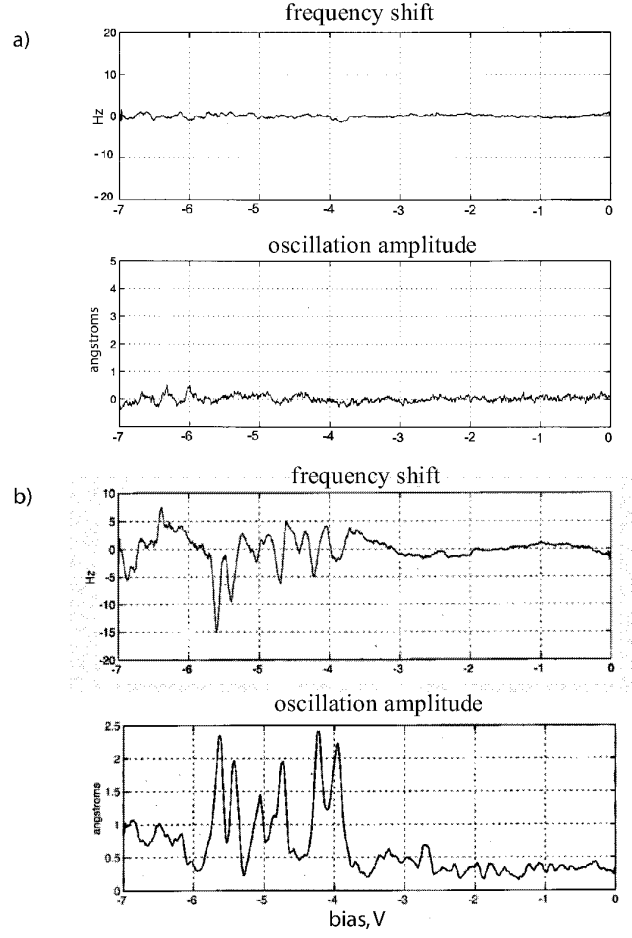


FIG. 9: Observation of localized states. a) Example of an EFS data with no signatures, b) on a site where there are localized states as evident from signatures.

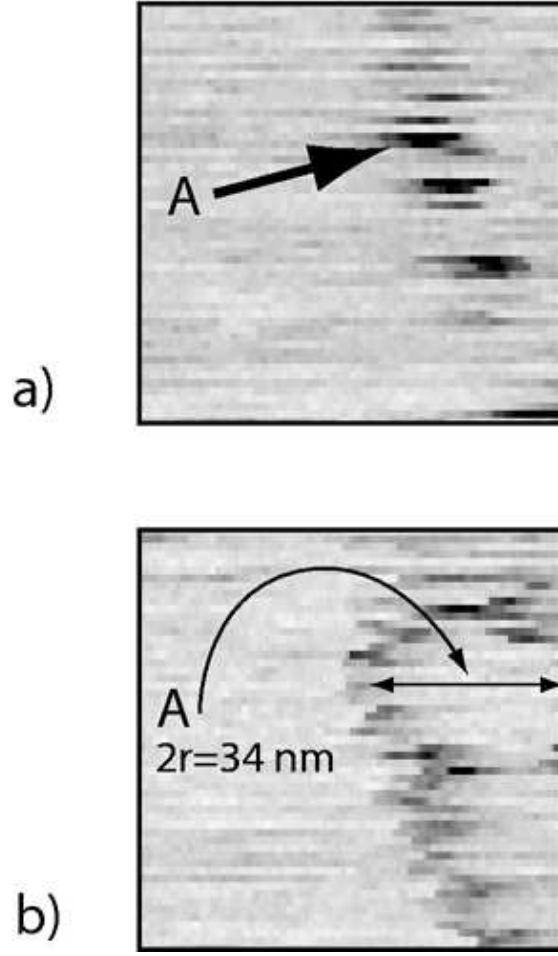


FIG. 10: Signature amplitude plotted as a function of x-y position of the tip in the vicinity of localized states. Tip height is $z_{ts}=20$ nm and the bias voltage is a) $V_{ts}=-4.45$ V, b) $V_{ts}=-5.15$ V. The signature located at point A first appears at $V_{ts}=-4.45$ V and has a radius of 17.3 nm at $V_{ts}=-5.15$ V. Theoretical estimate for the state, $h_i=14.5$ nm and $E_{i,0}=205$ meV correctly estimates the appearance and evolution of the signature.